Science Advances
AAAS

advances.sciencemag.org/cgi/content/full/6/27/eaba2735/DC1

Supplementary Materials for

Engineering bacterial outer membrane vesicles as transdermal nanoplatforms for photo-TRAIL–programmed therapy against melanoma

Li-Hua Peng*, Mao-Ze Wang, Yang Chu, Lei Zhang, Jie Niu, Hai-Tao Shao, Tie-Jun Yuan, Zhi-Hong Jiang, Jian-Qing Gao*, Xing-Hai Ning*

*Corresponding author. Email: lhpeng@zju.edu.cn (L.-H.P.); gaojianqing@zju.edu.cn (J.-Q.G.); xning@nju.edu.cn (X.-H.N.)

Published 3 July 2020, *Sci. Adv.* **6**, eaba2735 (2020)
DOI: 10.1126/sciadv.aba2735

The PDF file includes:

Other Supplementary Material for this manuscript includes the following:

(available at advances.sciencemag.org/cgi/content/full/6/27/eaba2735/DC1)

Table S1. Molecular interference of I-P-OMVs+NIR treatment in B16F10 cells

Cells behavior	Gene/Protein	Gene levels (/Blank control)	Protein levels (/Blank control)
Apoptosis	C-FLIP	1.9 ↓	7.5 ↓
	Survivin	1.4 ↓	5.1 ↓
	Bcl-2	1.6 ↓	
	Cleaved-Caspase 3		3.3 ↓
	Cleaved-Caspase 8		2.7 ↓
	Cleaved-PARP		6.3 ↓
Metastasis	E-Cadherin	1.4 ↓	2.8 ↑
	Vimentin	2.6 ↓	1.9 ↓
	MET (Cells)		1.5 ↓
	MET (OMVs)		3.7 ↓
	CAV-1 (Cells)		1.6 ↑
	CAV-1 (OMVs)		2.1 ↑
	Rab27A		1.5 ↓

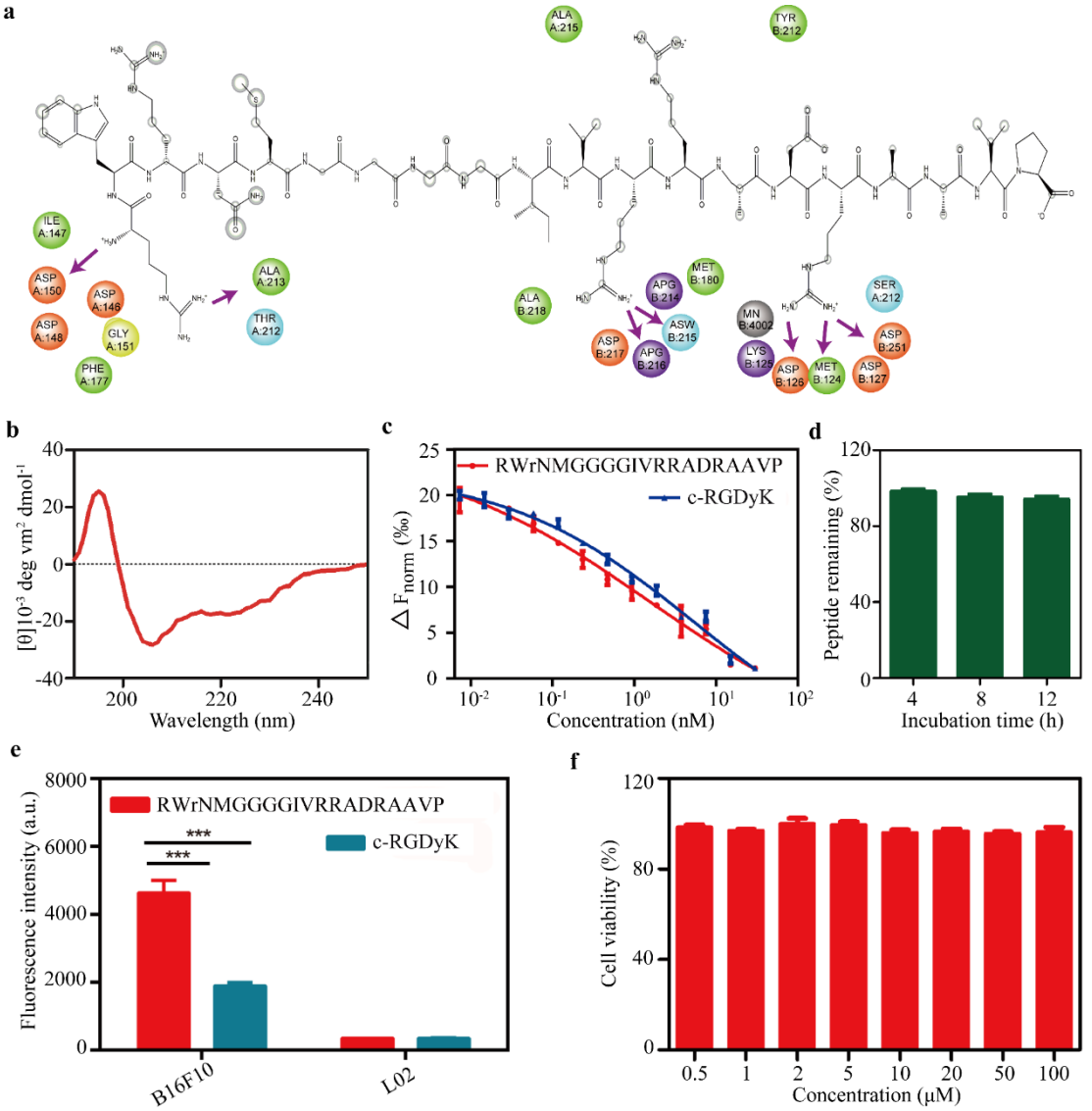

Fig. S1. Synthesis and characterization of αvβ3 integrin targeting peptides. a, Docking studies of RGP with integrin αvβ3. αv is labeled as chained A, and β3 is labeled as chained B. **b,** The circular dichroism spectrum of RGP. RGP forms α-heli. **c,** The Kd values of RGP and RGD with integrin αvβ3 measured by MicroScale thermophoresis. **d,** The stability of RGP in serum. **e,** The selective uptake of peptide candidates in B16F10 and L02 cells. **f,** The cytotoxicity of RGP in L02 cells. All data are represented as mean ± s.d. *** Indicates $p<0.001$.

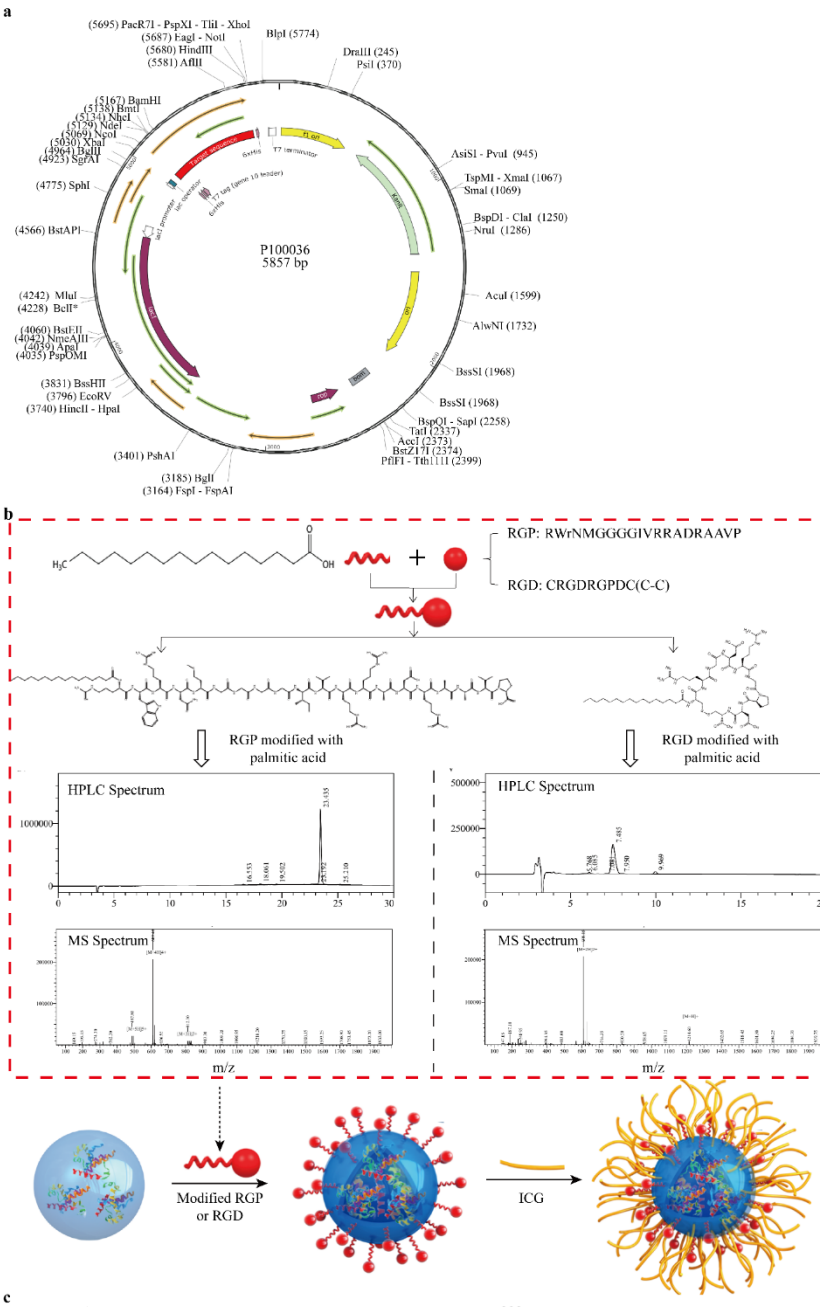
a
P100036
5857 bp
b
RGP: RWrNMGGGGIVRRADRAAVP
RGD: CRGDRGPDC(C-C)
RGP modified with palmitic acid
RGD modified with palmitic acid
HPLC Spectrum
MS Spectrum
m/z
Modified RGP or RGD
ICG
c
The concentration of TNF-α in cultural supernatants(pg/mL)
The concentration of IL6 in cultural supernatants (pg/mL)
1 ng/mL treated
10 ng/mL treated
PBS
LPS
I-OMVs
I-R-OMVs
I-P-OMVs
d
The concentration of TNF-α in skin (pg/mL)
The concentration of IL6 in skin (pg/mL)
0.5 mg/kg
0.75 mg/kg

Fig. S2. Map of plasmid DNA-TRAIL; synthesis and characterization of palmitic acid modified RGD and RGP peptides by LC-MS; schematic structures of I-R-OMVs, I-P-OMVs; inflammatory properties of I-P-OMVs *in vitro* & *in vivo*. a, The map of pDNA-TRAIL. **b,** Characterization of palmitic acid modified RGP and RGD by LC-MS analysis. The HPLC condition was: Buffer A: 0.1% TFA in 100% water(v/v), Buffer B: 0.1% TFA in 100% acetonitrile (v/v), Flow: 1 mL/minute, Wavelength: 214 nm, Column: SHIMADZU Inertsil ODS-SP (4.6*250MM*5UM). The MS conditions were optimized as: interface voltage, 4.5 kV; CDL temperature, 250 °C; CDL voltage, 0 V; block temperature, 200 °C; nebulizing gas, 1.5 L/minute; flow rate, 0.2 mL/minute. Schematic structures of I-R-OMVs and I-P-OMVs were also shown. **c,** TNF-α and IL-6 levels in the mice macrophage (RAW 264.7) treated by LPS, I-OMVs, I-R-OMVs, I-P-OMVs. **d,** TNF-α and IL-6 levels in the mice skin after intraperitoneal injection of LPS or topical application with I-OMVs, I-R-OMVs or I-P-OMVs. All data are represented as mean ± s.d. *** Indicates $p<0.001$.

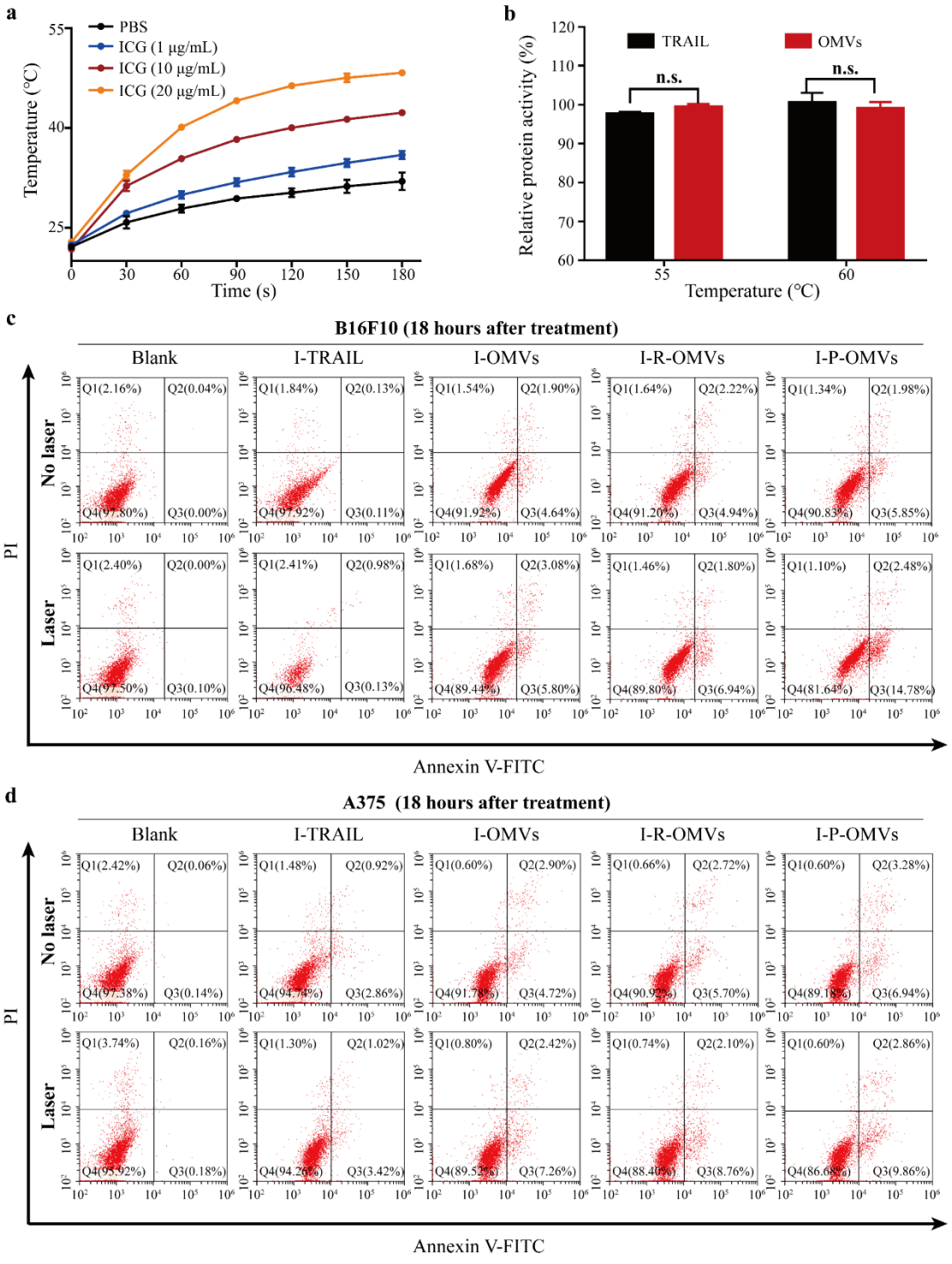

Fig. S3. PAP response induced by free ICG; stability of TRAIL in high temperatures; the influence of I-P-OMVs+NIR treatment in the apoptosis of B16F10 and A375 cells. a, Photo-thermal heating curves of ICG under 808 nm NIR laser irradiation at a power density of 2 W/cm^2 for 3 minutes (n=3). **b,** The activity of TRAIL at high temperatures (55 °C and 60 °C) (n=3). **c**, **d**, The influence of the different

OMVs+NIR on the apoptosis of B16F10 (**c**) and A375 (**d**), detected by Annexin V - FITC/PI staining. After incubated overnight, B16F10 and A375 cells were treated with the I-TRAIL, I-OMVs, I-R-OMVs, I-P-OMVs for 12 hours, then applied for NIR treatment (2 W/cm^2, 3 minutes), followed by the further 6 hours of incubation. Cells were harvested and the apoptosis of the cells were analyzed by a flow cytometer. The apoptosis in I-TRAIL+NIR, I-OMVs+NIR, I-R-OMVs+NIR and I-P-OMVs+NIR groups was enhanced with 1.3, 1.6, 1.5 and 1.9 folds, respectively than those groups without NIR irritation, suggesting that I-P-OMVs+NIR has a strong inhibitory effect to the activity of B16F10 or A375 cells. All blank group indicate cells treated by culture medium. All data are represented as mean ± s.d. n.s. indicates not significant.

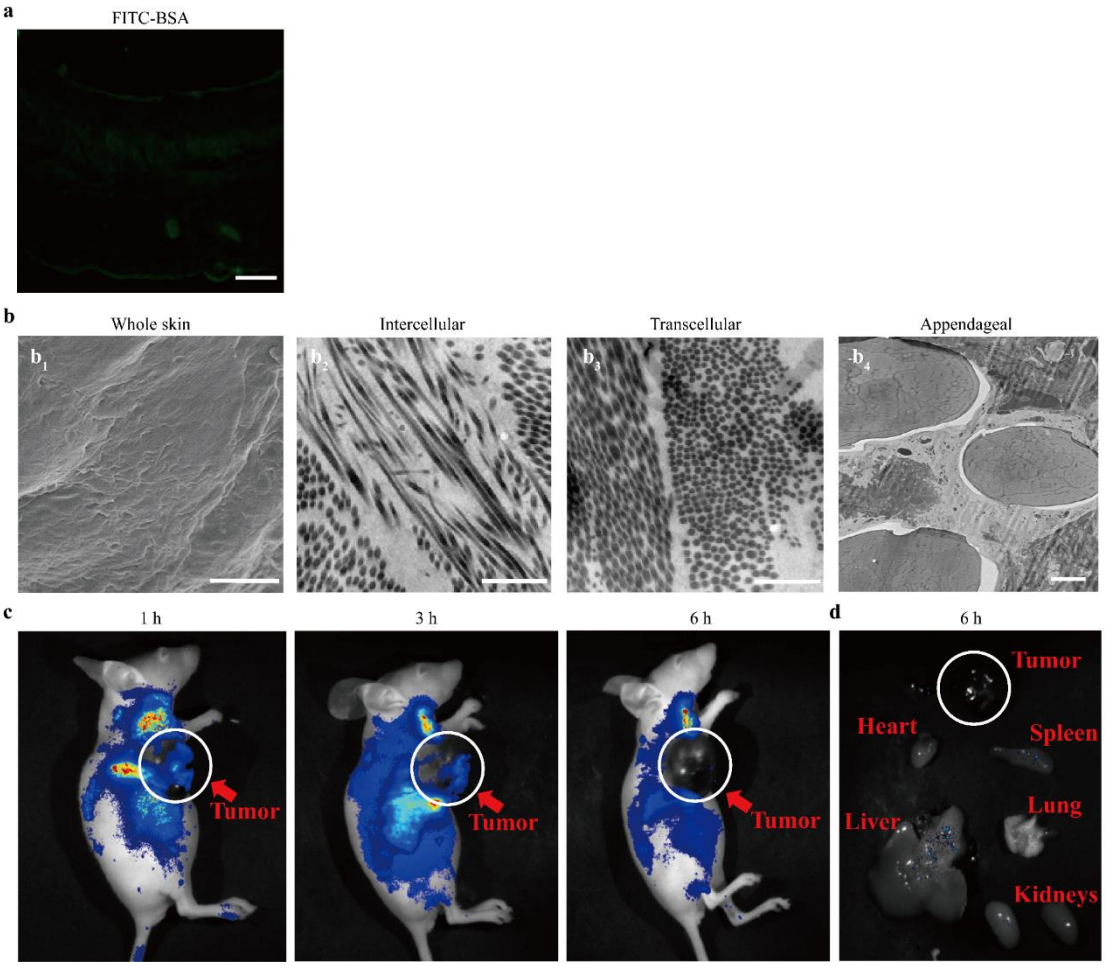

Fig.S4. Skin penetration of free FITC-BSA; SEM and TEM of blank skin; transdermal delivery of ICG *in vivo.* a, The distribution of FITC-BSA in skin slices after *in vitro* transdermal application for 6 hours. Scale bar, 100 μm. **b,** SEM image (b_1) and TEM images (b_2, b_3, b_4) of blank skin tissues without any treatment. No vesicle like structure can be observed in the normal skin slice. Scale bar, 1 μm. **c,** *In vivo* fluorescence imaging of tumor bearing mice at 1, 3, 6 hours after topical application of free Dil. **d,** Fluorescence image of the brain, heart, liver, spleen, lung and kidney harvested at 6 hours after treatment.

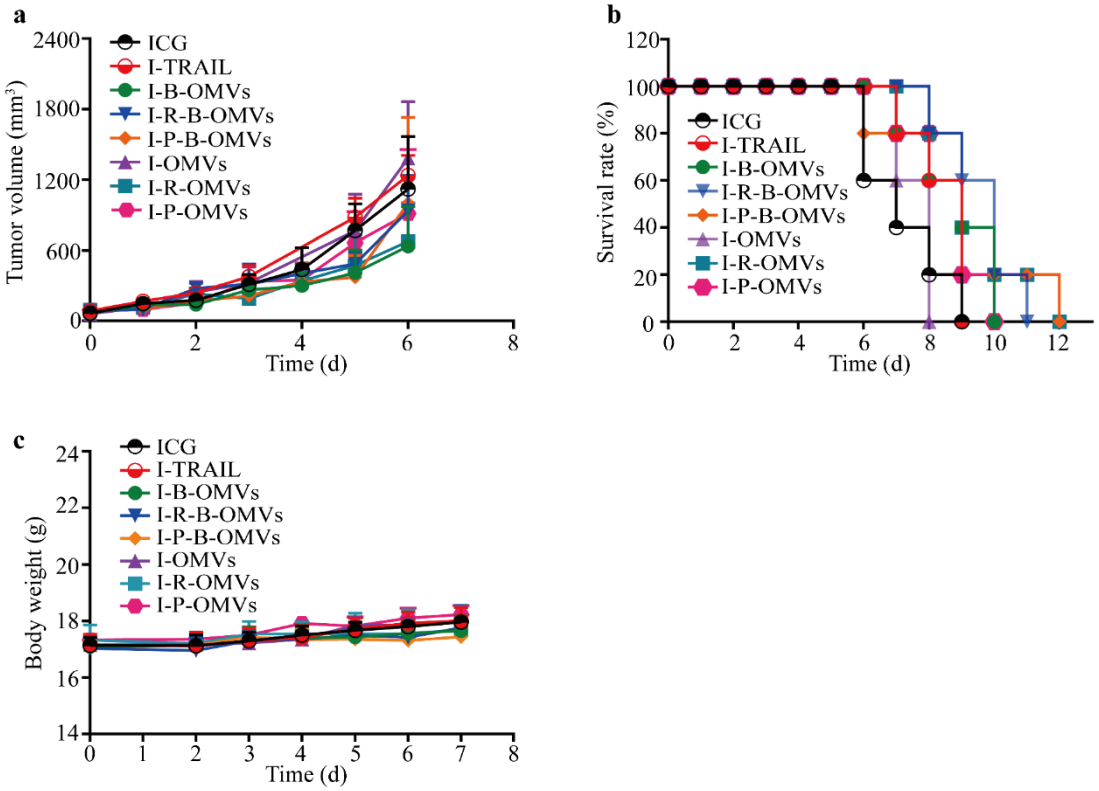

Fig. S5. Anti-tumor performance of the tested samples in C57BL/6J mice with grafted melanoma for 12 days (The first wave animal study). a, Tumor volumes of mice with xenograft tumors as a function of culture time after treatment. **b,** Survival rates of mice with xenograft tumors as a function of culture time after treatment. **c,** Body weight of mice with xenograft tumors as a function of culture time after first treatment. Compared with ICG group, all the tested regimens showed no significant influence in the progression of melanoma, which might be caused by the poor skin penetration of free TRAIL and the low sensitivity of melanoma to TRAIL. All data are represented as mean ± s.d. (n=6).

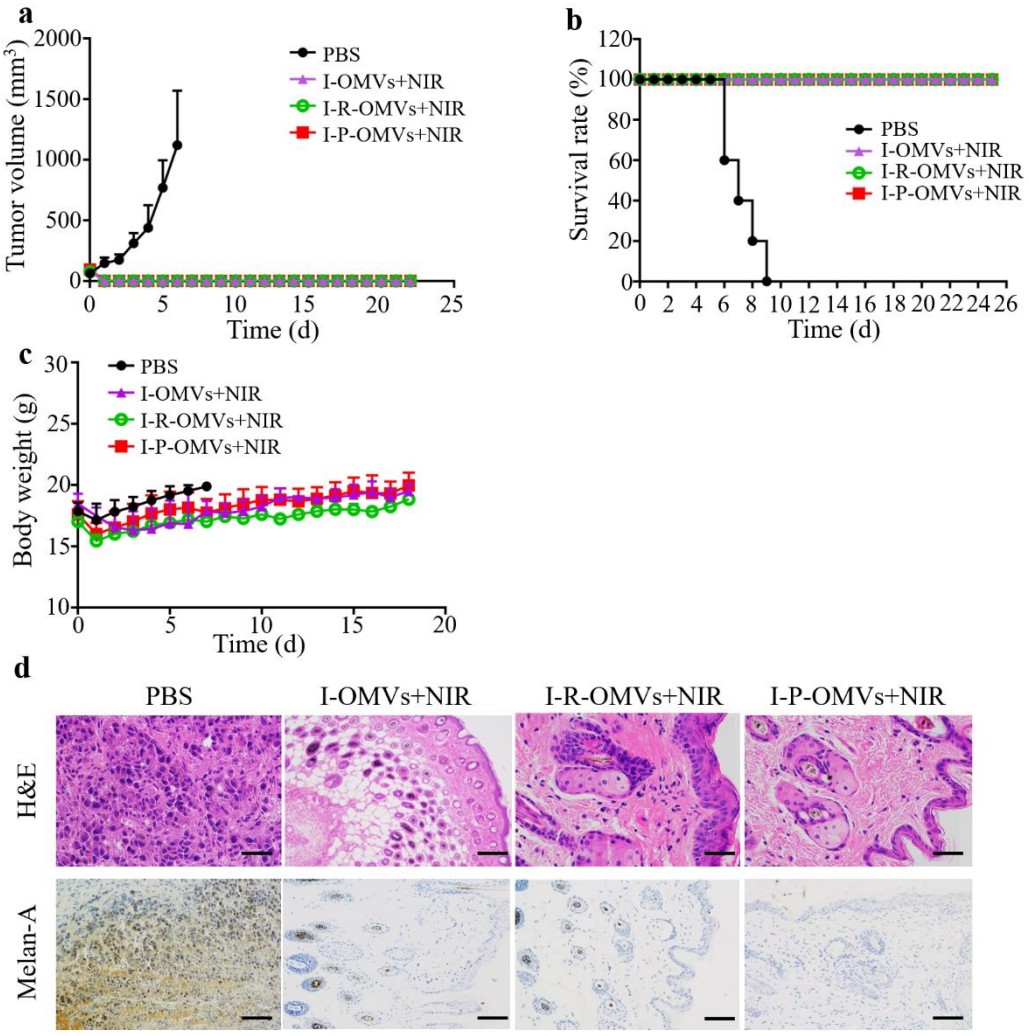

Fig. S6. Anti-tumor performance of the tested samples in C57BL/6J mice with grafted melanoma for 25 days (The third wave animal study). a, Tumor volumes of mice with xenograft tumors as a function of culture time after treatment. **b,** Survival rates of mice with xenograft tumors as a function of culture time after treatment. **c,** Body weight of mice with xenograft tumors as a function of culture time after first treatment. **d,** H&E and Melan-A staining of tumor tissues collected from tumor-bearing mice after treatment. With the increased intensity of NIR from 0.6 W/cm^2 to 2.0 W/cm^2, not only the tumors were cleared promptly, the tumor relapse was significantly retarded, and no observable tumors could be determined for at least 25 days. The topical tissue showed the morphology and histology of normal skin in the three kinds of OMVs+NIR treated groups. By contrast, tissues showed the morphology of melanoma in the blank control, which was confirmed by the identification of Melan-A. Consistent to results in

the previous treatments, strong Melan-A expression was shown in the PBS+NIR control group. For the I-OMVs+NIR, I-R-OMVs+NIR groups, some Melan-A expression can be observed. However, no Melan-A was detected in I-P-OMVs+NIR group. Scale bar, 50 μm. All data are represented as mean ± s.d. (n=6).

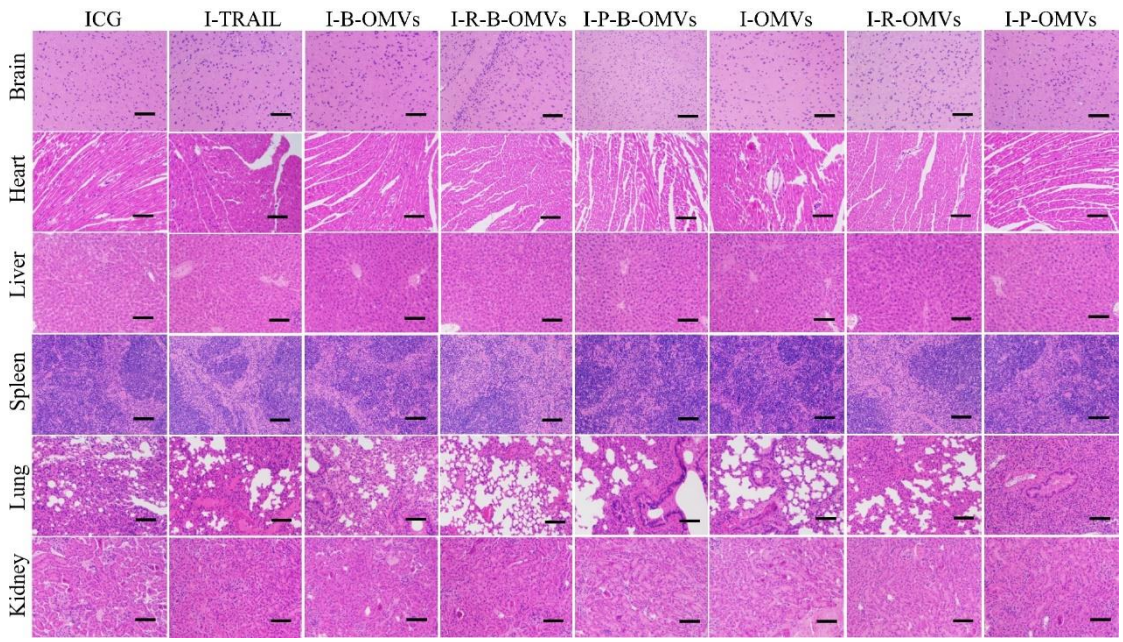

Fig. S7. H&E staining of organs slices of the mice with grafted melanoma on day 12 post-treatment (The first wave animal study). The organs, including brain, heart, liver, spleen, lung, and kidney were found to be normal in morphology, neatly arranged, and there was no infiltration of inflammatory cells and no obvious tissue damage, demonstrating the good biocompatibility of OMVs. Scale bar, 100 μm.

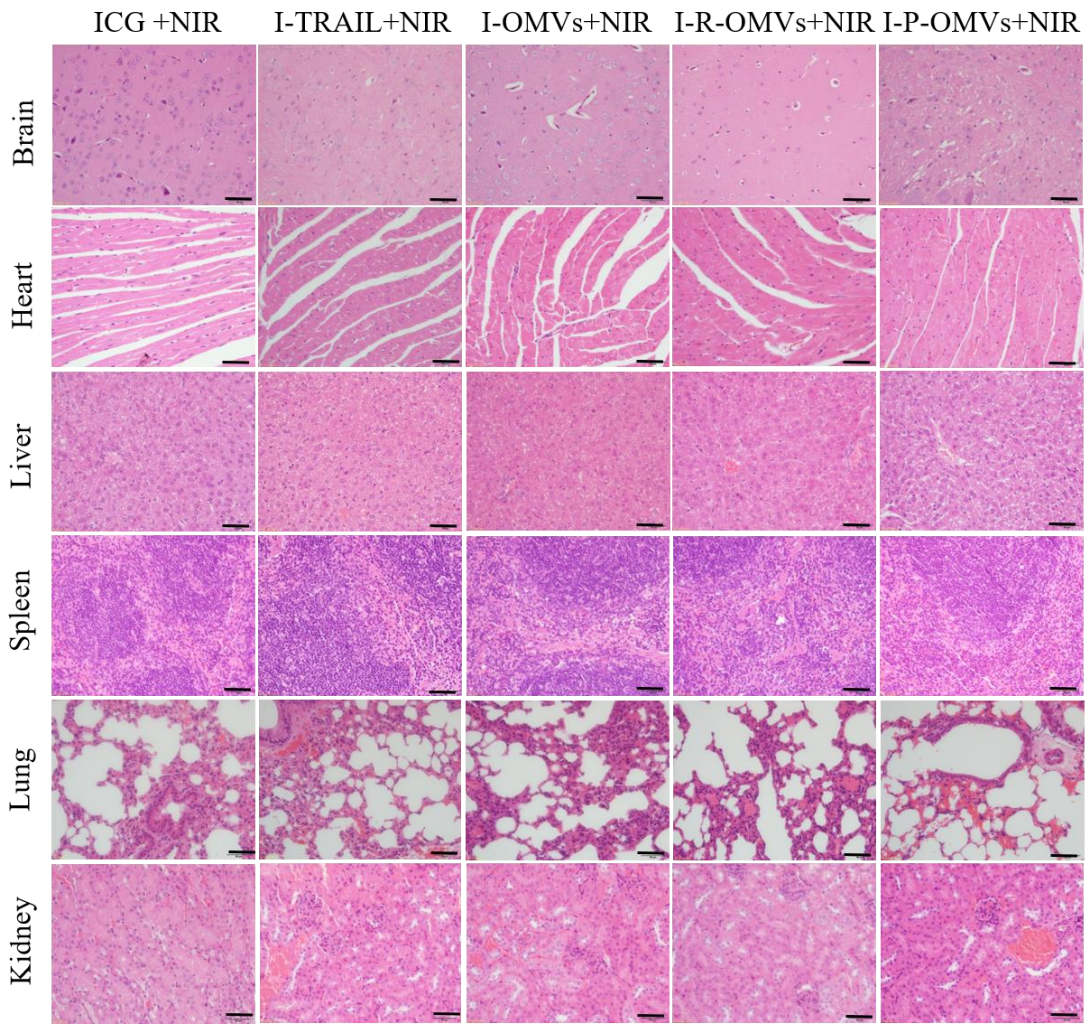

Fig. S8. H&E staining of organs slices of the mice with grafted melanoma on day 8 post-treatment (The second wave animal study). Tumor-bearing C57BL/6J mouse were topically treated by the tested samples for 12 hours, then irradiated by an 808 nm laser (0.6 W/cm^2) for 3 minutes. The organs, including brain, heart, liver, spleen, lung and kidney, were normal in morphology, neatly arranged, and there was no infiltration of inflammatory cells and no obvious tissue damage, demonstrating the good biocompatibility of OMVs. Scale bar, 100 μm.

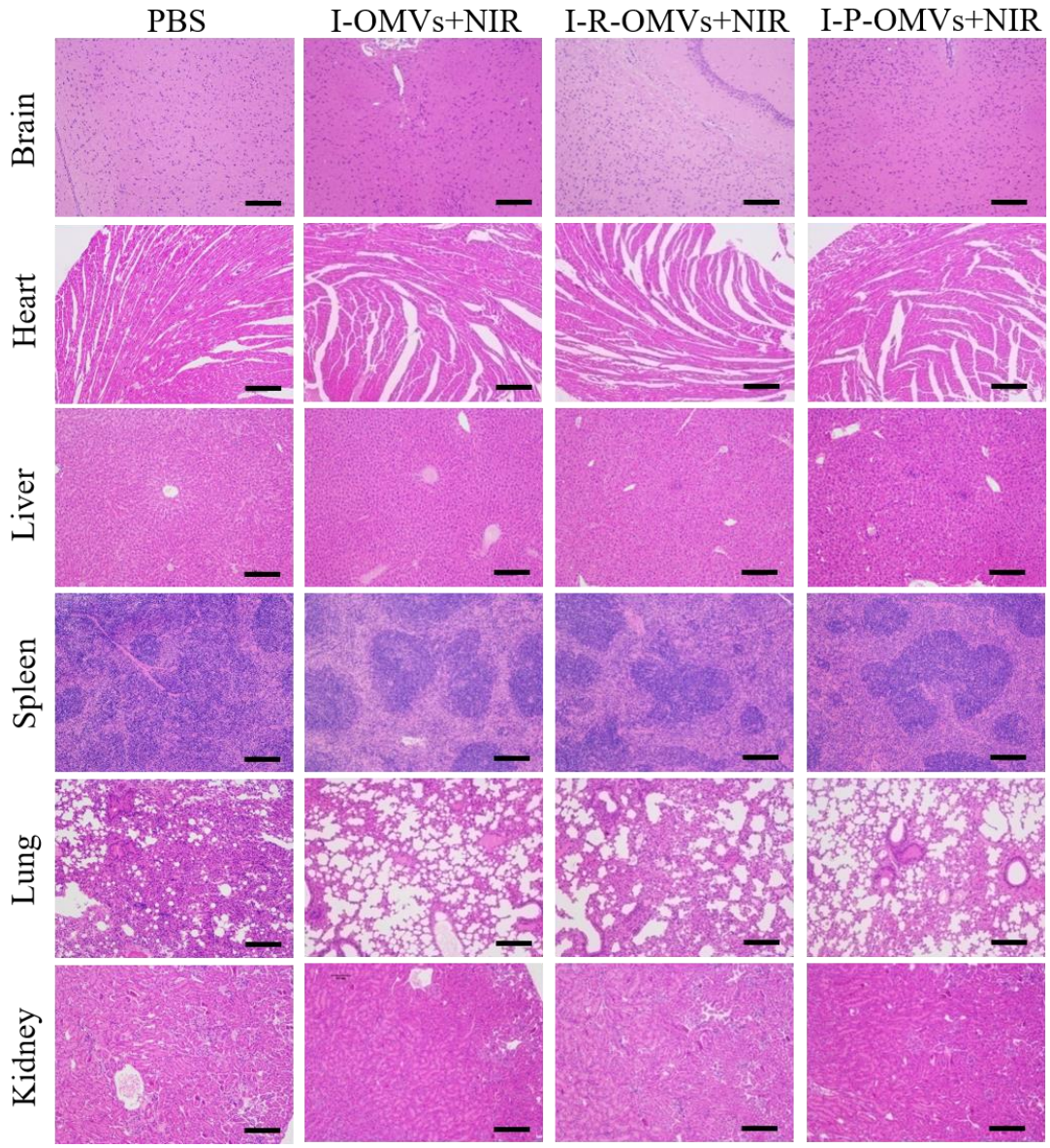

Fig. S9. H&E staining of organs slices of the mice with grafted melanoma on day 25 post-treatment (The third wave animal study). Tumor-bearing C57BL/6J mouse were topically treated by the tested samples for 12 hours, then irradiated by an 808 nm laser (2 W/cm^2) for 3 minutes. The organs, including brain, heart, liver, spleen, lung and kidney, were normal in morphology, neatly arranged, and there was no infiltration of inflammatory cells and no obvious tissue damage, demonstrating the good biocompatibility of the tested samples. Scale bar, 100 μm.

Video S1, The penetration of I-OMVs in the 3D melanoma spheroids.

Video S2, The penetration of I-R-OMVs in the 3D melanoma spheroids.

Video S3, The penetration of I-P-OMVs in the 3D melanoma spheroids.